creative commons
COMMONS DEED

저작자표시-동일조건변경허락 2.0 대한민국

이용자는 아래의 조건을 따르는 경우에 한하여 자유롭게

- 이 저작물을 복제, 배포, 전송, 전시, 공연 및 방송할 수 있습니다.
- 이차적 저작물을 작성할 수 있습니다.
- 이 저작물을 영리 목적으로 이용할 수 있습니다.

다음과 같은 조건을 따라야 합니다:

저작자표시. 귀하는 원저작자를 표시하여야 합니다.

동일조건변경허락. 귀하가 이 저작물을 개작, 변형 또는 가공했을 경우에는, 이 저작물과 동일한 이용허락조건하에서만 배포할 수 있습니다.

- 귀하는, 이 저작물의 재이용이나 배포의 경우, 이 저작물에 적용된 이용허락조건을 명확하게 나타내어야 합니다.
- 저작권자로부터 별도의 허가를 받으면 이러한 조건들은 적용되지 않습니다.

저작권법에 따른 이용자의 권리는 위의 내용에 의하여 영향을 받지 않습니다.

이것은 이용허락규약(Legal Code)을 이해하기 쉽게 요약한 것입니다.

Disclaimer

dCollection

ULSAN NATIONAL INSTITUTE OF
SCIENCE AND TECHNOLOGY

Mono-layered Photonic Crystal Patterning for Anti-counterfeit Applications of Structural Colors

Hyunmoon Nam

Department of Mechanical Engineering

Graduate School of UNIST

2015

ULSAN NATIONAL INSTITUTE OF
SCIENCE AND TECHNOLOGY

Mono-layered Photonic Crystal Patterning for Anti-counterfeit Applications of Structural Colors

Hyunmoon Nam

Department of Mechanical Engineering

Graduate School of UNIST

ULSAN NATIONAL INSTITUTE OF
SCIENCE AND TECHNOLOGY

Mono-layered Photonic Crystal Patterning for Anti-counterfeit Applications of Structural Colors

A thesis
submitted to the Graduate School of UNIST
in partial fulfillment of the
requirements for the degree of
Master of Mechanical Engineering

Hyunmoon Nam

12. 09. 2014
Approved by

Thesis Chair: Taesung Kim

ULSAN NATIONAL INSTITUTE OF
SCIENCE AND TECHNOLOGY

Mono-layered Photonic Crystal Patterning for Anti-counterfeit Applications of Structural Colors

Hyunmoon Nam

This certifies that the thesis of Hyunmoon Nam is approved.

12. 09. 2014

Thesis Chair: Prof. Taesung Kim

Thesis Committee Member: Dr. Kyungjun Song

Thesis Committee Member: Prof. Myounghoon Song

ULSAN NATIONAL INSTITUTE OF SCIENCE AND TECHNOLOGY

Abstract

Photonic crystals (PCs) can manipulate electromagnetic wave by designing artificial periodic dielectrics, which provides various applications such as sensor, LED, laser, and optical computers. Recently, many studies focus on display applications by designing photonic band-gap while the fabrication of photonic crystals in a nanoscale is still challenging. In this work, a simple method is described for fabricating mono-layered self-assembled photonic crystals (SAPCs) by using inkjet material printers that are able to inject nanoparticle suspension on a substrate in contrast to conventional approaches such as photo-lithography, two-photon patterning, and direct-write assembly. For making homogeneous single-layered structure, crucial factors influencing the micro-patterns of a colloidal assembly of the inkjet-printed droplet were investigated including the substrate wettability and chemical composition of ink to see what effect they might have on producing structure color. These patterned photonic crystals yield stealth ability to avoid pattern detection from counterfeiters under day light illumination and generate multiple colorful holograms on different viewing angles for complex cryptography. In addition, the number of SAPCs in a matrix format controls optical intensities, thus yielding extra anti-counterfeiting function. Because the inkjet-printed-based SAPC platforms provides a simple and the unique optical properties, it is believed that the approach can be widely used for anti-counterfeiting systems.

ULSAN NATIONAL INSTITUTE OF SCIENCE AND TECHNOLOGY

Table of Contents

ULSAN NATIONAL INSTITUTE OF SCIENCE AND TECHNOLOGY

List of Figures

ULSAN NATIONAL INSTITUTE OF SCIENCE AND TECHNOLOGY

ULSAN NATIONAL INSTITUTE OF SCIENCE AND TECHNOLOGY

ULSAN NATIONAL INSTITUTE OF SCIENCE AND TECHNOLOGY

Chapter 1 Introduction

1.1 Motivation

Anti-counterfeiting techniques are essential technologies in order to identify the authentication of products. However, recent advance of fabrication and information technology easily counterfeits products to be seen identical compared to original products. Photonic crystals[1, 2] yield promising routes for manipulating light spectrum and intensity at will, showing remarkable potential for defending against highly sophisticated counterfeiting techniques[3-5]. The control and manipulation of spectroscopic information can be obtained by photonic band-gap designed by periodic multi-layered nanostructures[1, 2] and using external stimulus such as temperature[6], mechanical stretching[7], solvent[8], and electromagnetic field[9, 10]. Higher dimensional photonic crystals are generally fabricated by photo-lithography[11, 12], two-photon patterning[13, 14] and direct-write assembly[15, 16], but these fabrications require complicate processes, inefficient time and labor, and expensive equipment[11-17]. To overcome the disadvantages aforementioned, in this work, a commercially available materials printer [18-20] is used to design a novel and durable anti-counterfeiting technique, relying on mono-layered self-assembled photonic crystals (SAPCs).

These patterned photonic crystals are stealthy and thus, can avoid pattern detection by counterfeiters in daylight. The crystals also generate multiple colorful holograms at different viewing angles for complex cryptography. In addition, the number of SAPCs in a matrix format controls optical intensities, thus yielding an extra anti-counterfeiting function. The printed photonic-crystal platforms show a practical significance in the authentication of invaluable and commercial products.

ULSAN NATIONAL INSTITUTE OF SCIENCE AND TECHNOLOGY

1.2 Structure of the Thesis

There are four chapters in the thesis. Chapter 1 will briefly give an overview of the content of the thesis. Chapter 2 will present background and literature review of inkjet printing technology and photonic crystal for cryptography. Chapter 3 will discuss ink formulation, ink-substrate system, and pattern formation to fabricate SAPCs printed from aqueous suspensions of nanosilicas. Based on these, Chapter 4 will demonstrate characteristic of SAPCs and practical application of photonic crystal patterns for anti-counterfeiting system.

1.3 Characterization Techniques

We used a piezoelectric drop on demand inkjet printer manufactured by Fujifilm Dimatix, Inc. (DMP-2800, CA, USA), with a cartridge (Model no. DMC-11610) that supports 10 pL droplets, which were used in all of the experiments[21]. The contact angle (CA) of various substrates was measured by gently dropping deionized water droplets of 2 μL onto the various substrates and then by using a goniometer equipped with an optical system and a CCD camera (Model 200, Ramé-Hart Instrument Co., Succasunna, NJ, USA). All the CA reported in this study have been averaged from at least 10 measurements. Scanning electron microscope (SEM) images were taken and utilized to study the morphology and spatial distribution of the deposited silica (S-4800, Hitachi, Japan). Micrographs were taken by using a high resolution CCD camera (Eclipse 80i, Nikon, Japan). We used two types of CCD cameras: a SLR CCD camera (Nikon D300, Pentax K-x) for high quality images and a webcam for regular images. Optical intensity and RGB histogram were obtained from the Image J. Camera positions were carefully manipulated by using a custom zig setup. Spectra were measured by using a spectrophotometer (Cary 5000 UV-vis-NIR, Santa Clara, CA, USA).

ULSAN NATIONAL INSTITUTE OF SCIENCE AND TECHNOLOGY

Chapter 2 Background and Literature Review

2.1 Inkjet Printing Technology

2.1.1 Inkjet printing techniques

Inkjet printing is direct-write techniques for depositing and patterning materials in the fluid on a substrate and it can be used for wide range of materials including metals, ceramics and polymers for many different applications. Although conventional photolithography has been generally used for fabricating micro/nano patterns, it involve complicated processes and require efficient time management and labor, as well as expensive equipment. In contrast, because inkjet printing are simple, fast and provide non-contact and mask-less method, this approach is considered as a promising alternative to traditional lithography[22, 23].

Inkjet printing involves the production of tiny drops of fluid and the droplet position in precise locations on a substrate. There are various methods for drop generation, but it can be classified into two large groups as continuous inkjet (CIJ) and drop on demand inkjet (DOD). CIJ expels drops constantly from a print head and is primarily used for some graphic applications such as marking and labeling. On the other hand, DOD inkjet ejects droplets from the print head only when necessary. DOD method is a suitable approach for forming patterns because this technique provides high placement accuracy leading to high resolution of printed patterns, controllability, and efficient use of materials[24].

DOD mode can be classified in thermal DOD and piezoelectric DOD (Fig. 2.1). In a thermal DOD inkjet printer, ink is heated until a vapor bubble is created to eject an ink droplet. Since thermal DOD involves the vaporization of the ink inside the chamber, the ink must have a volatile solvent, allowing for the vapor bubble[25].

In case of piezoelectric DOD, the ejection of the droplet is caused by the mechanical deformation of a piezo-crystal when a voltage is applied. For this reason the piezo-based inkjet is applicable to a wider

ULSAN NATIONAL INSTITUTE OF SCIENCE AND TECHNOLOGY

variety of inks than thermal inkjet because a volatile solvent is no requirement to form ink droplet. Therefore piezoelectric inkjet printing method is widely adopted for patterning[24, 26].

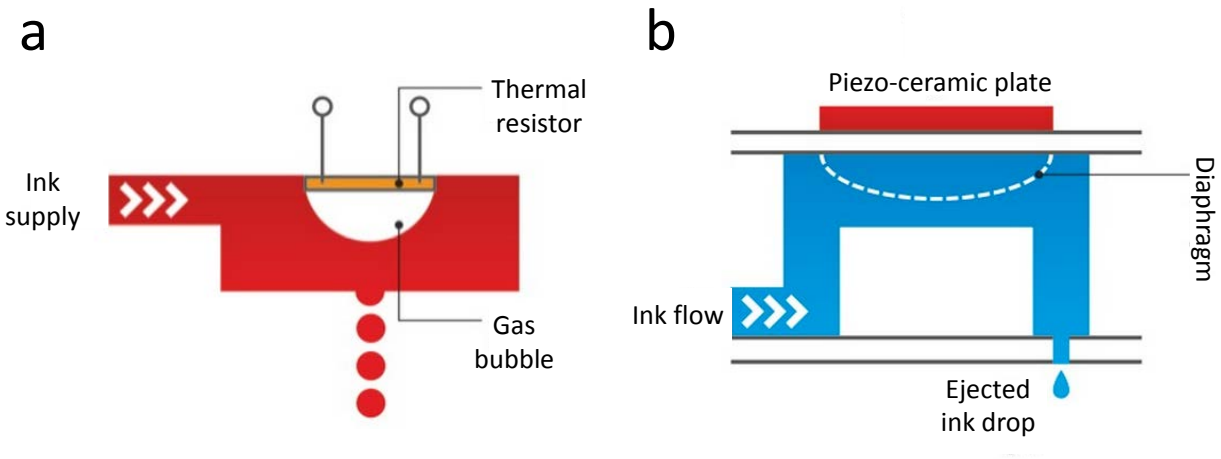

Fig. 2.1 Schematic illustration of continuous ink jet (left) and piezoelectric drop on demand ink jet (right)[27].

2.1.2 Required properties of inks

The formulation of suitable inks is critical part for inkjet printing because the ink and its viscosity and surface tension determine the ejection characteristics of droplets and the pattern quality[23]. However, the formulation for ink depends on the printer used and the material to be printed. Typically, the ink should have a viscosity of 10-12 mPas[28]. In case of the surface tension that is influence on the shape of the drop, typical values of surface tension ranges from 28 mNm^{-1} to 32 mNm^{-1}[28]. Besides, the time-stability of the suspension is important parameter because the particles in suspension have to maintain uniform dispersion without aggregation for all the time of the printing process.

ULSAN NATIONAL INSTITUTE OF SCIENCE AND TECHNOLOGY

2.2 Photonic Crystal for Encoding

Photonic crystals are periodic nanostructures that can cause diffraction and reflection at certain specific wavelengths perceived as color by the human eye[29]. The control and manipulation of spectroscopic information can be achieved by various ways such as electromagnetic fields, solvents, and laser induced periodic surface for encoding.

Hu et al. demonstrate photonic paper composed of magnetically induced self-assembly of superparamagnetic colloidal nanoparticles (Fig. 2.2a)[30]. The paper features toggle effect (show or hide) caused by application and withdraw of a magnetic field.

Fig. 2.2b shows technique for chemical encipherment in 3D-ordered porous photonic crystal with inverse opal structure[9]. The message, W-INK, is encoded using four different chemistry (trimethylsilyl, 3,3,3-trifluoropropylsilyl, n-decylsilyl, and 13FS). Unable verify the pattern in the air, but four different words can be displayed when immersed in ethanol (EtOH). In other words, the different words appear according to the concentration of ethanol.

Fig. 2.2c presents laser induced periodic surface structures (LIPSS) formed by applying ultra-short pulse (e.g. femtosecond laser)[31]. Because periodic surface structures, usually named ripples, act as diffraction grating, a color effect can be obtained when white light is illuminated on the surface. However, it is impossible to exhibit the colors if direction of white light is parallel to the ripples: there is no interference between light and ripples. As a result, the colors can be selectively produced, depending on a relation between light direction and ripple orientation.

ULSAN NATIONAL INSTITUTE OF SCIENCE AND TECHNOLOGY

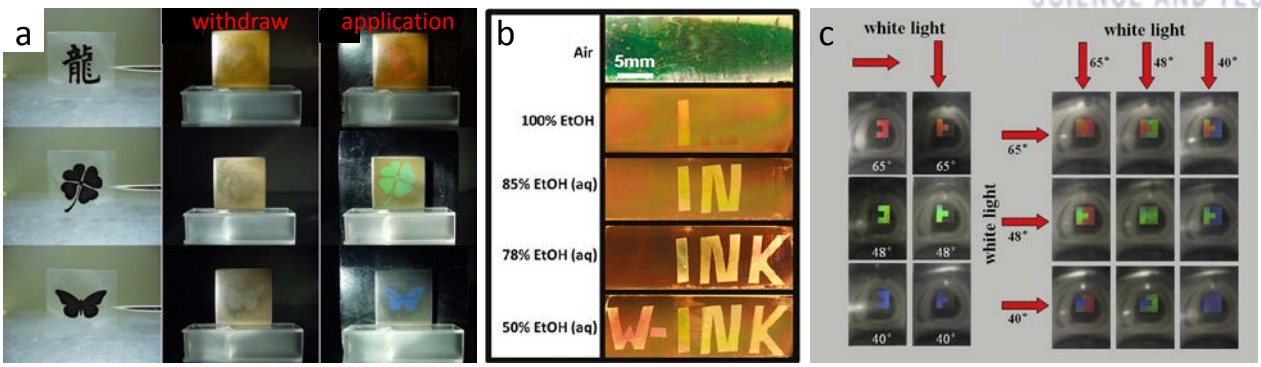

Fig. 2.2 **a-c**, Various methods to manipulate spectroscopic information of photonic crystal for encoding. (a) Electromagnetic fields, (b) solvents, (c) laser induced periodic surface.

ULSAN NATIONAL INSTITUTE OF SCIENCE AND TECHNOLOGY

Chapter 3 Experimental

3.1 Printing of Nano Silica Suspension

3.1.1 Material printer system

The inkjet printer used for the fabrication of patterned photonic crystal in this thesis is the Dimatix Materials Printer 2800 (DMP2800), a software controlled DOD printer using a piezo-based inkjet cartridge. (Fig. 3.1). A printer head consists of 16 nozzles in a row with a 254 μm spacing distance. Each nozzle is approximately 21.5 μm in diameter and its operation can be controlled individually. The center-to-center drop spacing is adjustable between 5 and 254 μm in one micron increments and depends on the dpi setting. The 5 μm drop spacing corresponds to a 5080 dpi printing resolution as a maximum, while 254 μm corresponds to 100 dpi as a minimum. We mainly used 254 dpi, which meant a drop spacing of 100 μm, which is appropriate distance to prevent overlapping between droplets[21].

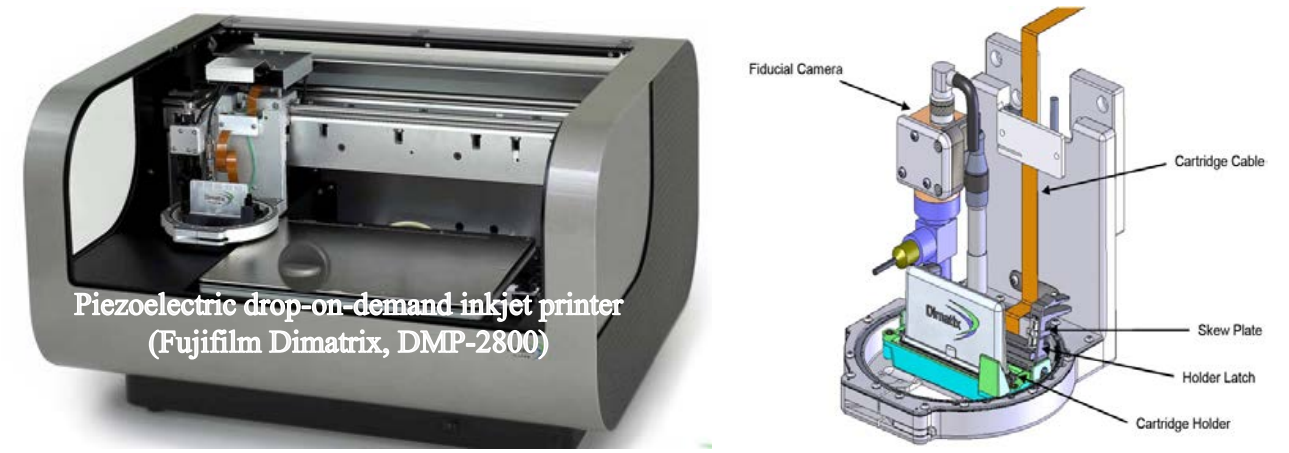

Fig. 3.1 Photograph of Dimatix Materials Printer (DMP-2800) and schematics of print cartridge of DMP 2800.

ULSAN NATIONAL INSTITUTE OF SCIENCE AND TECHNOLOGY

3.1.2 Preparation of SiO_2 suspension inks

Monodisperse plain silica particles (10% w/v) with diameters of 400 nm and 500 nm (Polysciences, Warrington, USA) were used. To manipulate the final working concentration of the particles, the following centrifugal steps were employed. First, a 1000 μL solution of silica particles as delivered was centrifuged at 4000 rpm for 12 minutes, and then the solution was removed for a high concentration particle suspension (> 20% w/v) or diluted with deionized water for a low concentration particle suspension (< 10% w/v). Next, the particle suspension was mixed with FA (Sigma Aldrich, Korea) in a ratio of 4 to 1 in volume to control evaporation time for better self-assembly[18]. The prepared, mixed particle suspension was treated ultrasonically for 10 minutes for complete dispersion (5510E-DTH, Bransonic, USA).

3.1.3 Substrate pretreatments

A surface property of the substrate is another important factor to achieve uniform deposition. Four different substrates were used to investigate effects of hydrophobicity and hydrophilicity of substrates on crystallization of nano silica suspension such as slide glass, Si-wafer, polydimethylsiloxane (PDMS), polypropylene (PP) and the substrates were cut by a diamond knife. All substrates were carefully cleaned in acetone and IPA, rinsed with deionized (DI) water, and then dried with nitrogen gas. No further surface modification was made.

ULSAN NATIONAL INSTITUTE OF SCIENCE AND TECHNOLOGY

3.2 Patterns from Inkjet Printing

3.2.1 Formation of dot and line pattern

The inkjet-printed patterns can be divided into two major sections as dot and line pattern. Even though this is just simple patterns, it is essential basis to fabricate various and complicated patterns. Fig. 3.2 shows the patterns of dots and lines printed using SiO_2 suspension inks 1% (w/v) on a hydrophilic (slide glass) and hydrophobic substrate (PDMS). Diameter of printed dot on slide glass was around 70 μm, while each dot in diameter of around 7 μm was printed on PDMS. We were able to obtain dot and continuous line patterns on slide glass by controlling a droplet spacing, which means dot to dot distance (Fig. 3.2a)[23]. When the droplet spacing exceeds the diameter of the printed dot, single dot pattern was generated. In contrast, narrowing droplet interspacing results in merging of individual droplet on hydrophilic substrate. As a result, when the droplet spacing reduces below the diameter of the single dot, continuous lines formed. In case of hydrophobic substrate, the formation of continuous lines is difficult to achieve because of the strong de-wetting caused by the substrate as shown in Fig. 3.2b.

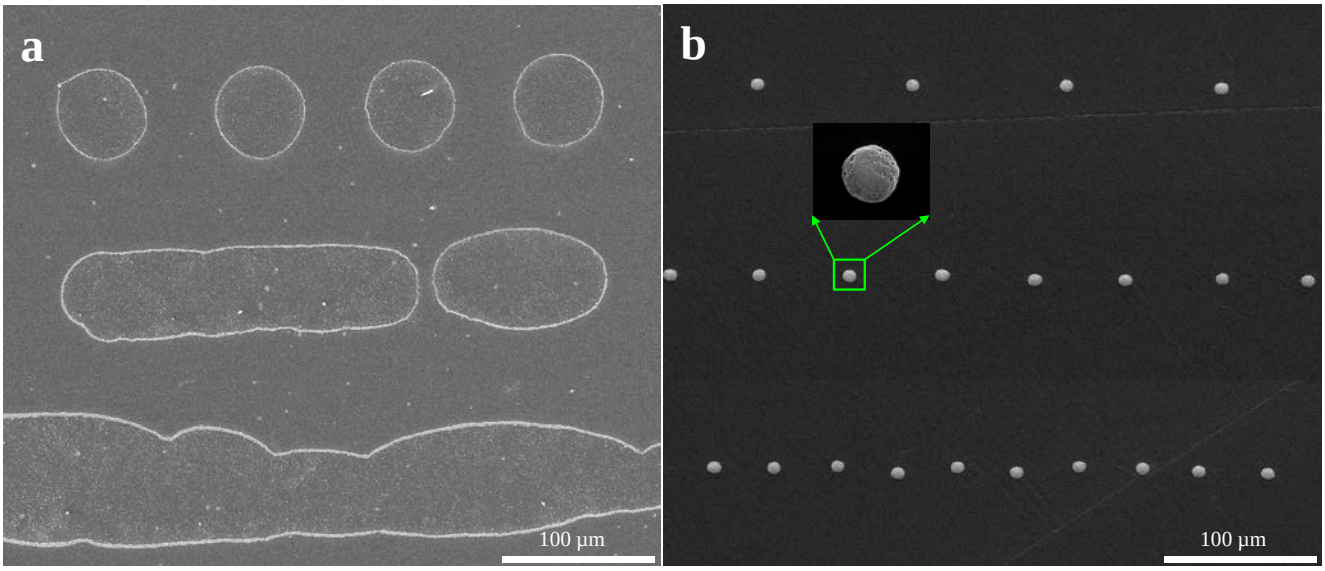

Fig. 3.2 The formation of dot and line pattern by controlling a droplet spacing in hydrophilic and hydrophobic surface **a**, SEM images of ink-jet printed patterns as a function of droplet interspacing in hydrophilic surface: 100 μm, 60 μm, 40 μm **b**, SEM images of ink-jet printed patterns as a function of droplet interspacing in hydrophobic surface: 100 μm, 60 μm, 40 μm

ULSAN NATIONAL INSTITUTE OF SCIENCE AND TECHNOLOGY

3.2.2 Behavior of a droplet on the substrate

Fig. 3.3 shows a basic physics of an inkjet printing process for producing droplet patterns on a hydrophilic and hydrophobic substrate, respectively. Injected particles with 500 nm are used to form photonic crystals by drying process. As soon as suspension was injected on the surface, it seems to spread out due to the momentum of the droplet. We employed a hydrophilic (glass) and hydrophobic (PDMS) substrate printed with 10% (w/v) water-based nanobead suspension. In case of hydrophilic surface, the water-based droplet becomes asymmetric due to high surface energy: the edge of the droplet becomes thin, while the center becomes relatively thicker (Fig. 3.3a). Since an evaporation rate at the edge is much faster than center region in droplet, a capillary flow is generated to replenish a fluid at the edge. As a result, the particles are transported to the edge by outward flow and produced a coffee-ring-shaped pattern in which several nanobead layers were self-assembled only along the perimeter (Fig. 3.3c-i)[32].

In contrast, the same nanobead suspension was repeatedly injected on the PDMS substrate and the self-assembled nanobead structures were dome-shaped as shown in Fig. 3.3b. The hydrophobic surface appears to make the injected area shrink. As a result, the surface area of the self-assembled, dome-shaped nanostructure is much smaller than on hydrophilic surface (Fig. 3.3c-ii).

ULSAN NATIONAL INSTITUTE OF
SCIENCE AND TECHNOLOGY

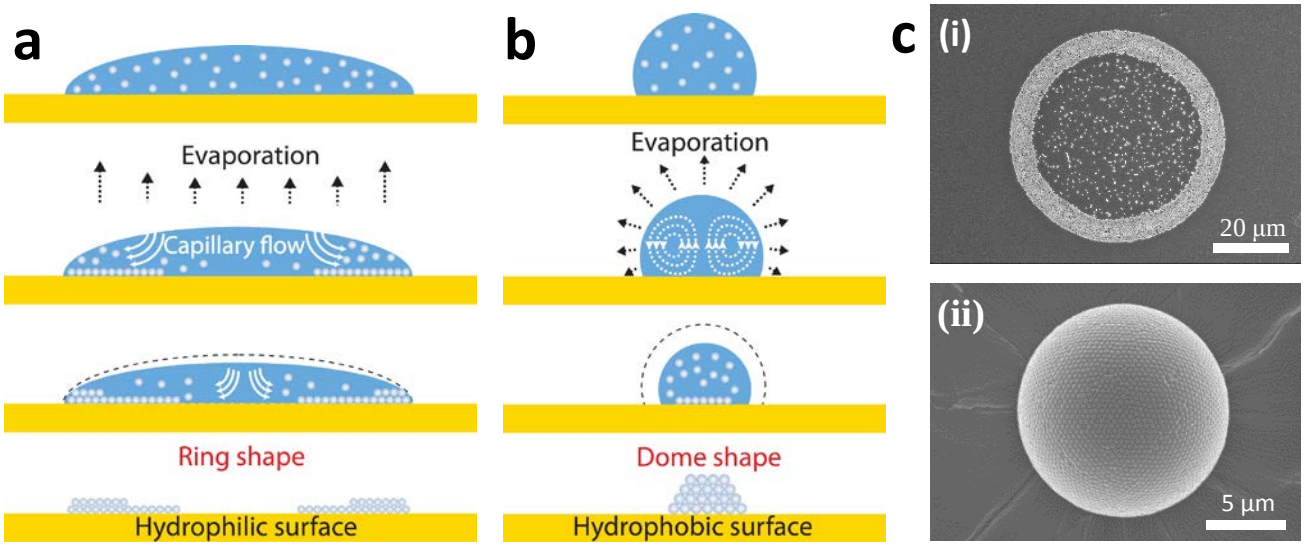

Fig. 3.3 **a-b**, Schematic of evaporation process in a droplet and different nanostructures on hydrophilic and hydrophobic surfaces. **c**, SEM images show (i) a ring-shaped and (ii) a dome-shaped nanostructure.

ULSAN NATIONAL INSTITUTE OF SCIENCE AND TECHNOLOGY

3.2.3 Mono-layered, self-assembled structure using Marangoni effect

In order to obtain mono-layered structure, several experiments were designed to examine surface wettability, the concentration of nanobeads, and effects of solvents as shown in Fig. 3.4a. First, water-based two nano-bead suspensions at 10% (w/v) and 20% (w/v) on a hydrophilic glass with contact angle 10° were studied. Both of them produced a coffee-ring shape pattern. Second, the same nanobead suspension (10% (w/v), 20% (w/v)) with 100 μL formamide (FA) as drying control agent on a hydrophilic glass[18]. In this case, a low concentration suspension 10% (w/v) also formed ring pattern, but a high concentration suspension (20% w/v) produced a monolayer pattern. This means manipulating both the solvent system and the number density of silica particles enabled mono-layered structure on hydrophilic substrates. In fact, these results indicate that solvent system (water/FA mixture) is more crucial than concentration to control the evaporation time and make a homogeneous single layer: FA has higher boiling point than water, while water has higher surface tension than FA.

When using solvents that contained water/FA mixture, the water preferentially evaporated at the edge. As a result, capillary fluid movement occurs from center to edge in droplet. However, the resulting surface tension gradient induces Marangoni flow from the edge to the center because the FA concentration is higher near the perimeter, which reduces the surface tension[18, 33]. Therefore, this flow can balance the capillary flow and we can achieve uniform deposition. Fig. 3.4b shows SEM images of self-assembled, mono-layered photonic crystal dots on a glass substrate (i–ii). Each dot is about 70 μm in diameter (i) and comprised of the nano-sized silica particles (ii).

ULSAN NATIONAL INSTITUTE OF
SCIENCE AND TECHNOLOGY

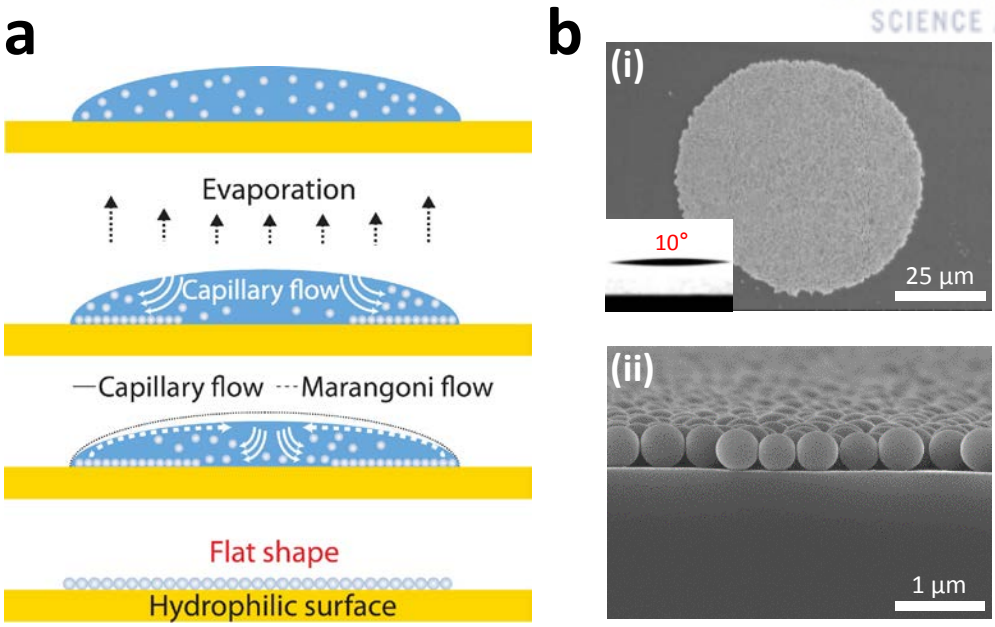

Fig. 3.4 **a**, Schematic of evaporation process in a droplet for producing monolayer nanostructure. **b**, SEM images show (i) a mono-layered nanostructure and (ii) a cross section view of single layer.

ULSAN NATIONAL INSTITUTE OF SCIENCE AND TECHNOLOGY

3.2.4 Multiple injection on glass and PDMS

We also tried multiple injection on glass and PDMS respectively. In case of glass, the number of layers piled on glass are almost equal to the number of injection (Fig. 3.5a). On the other hand, Fig. 3.5b shows that the size of dorm-shaped structure on PDMS grow bigger as the number of injection increases.

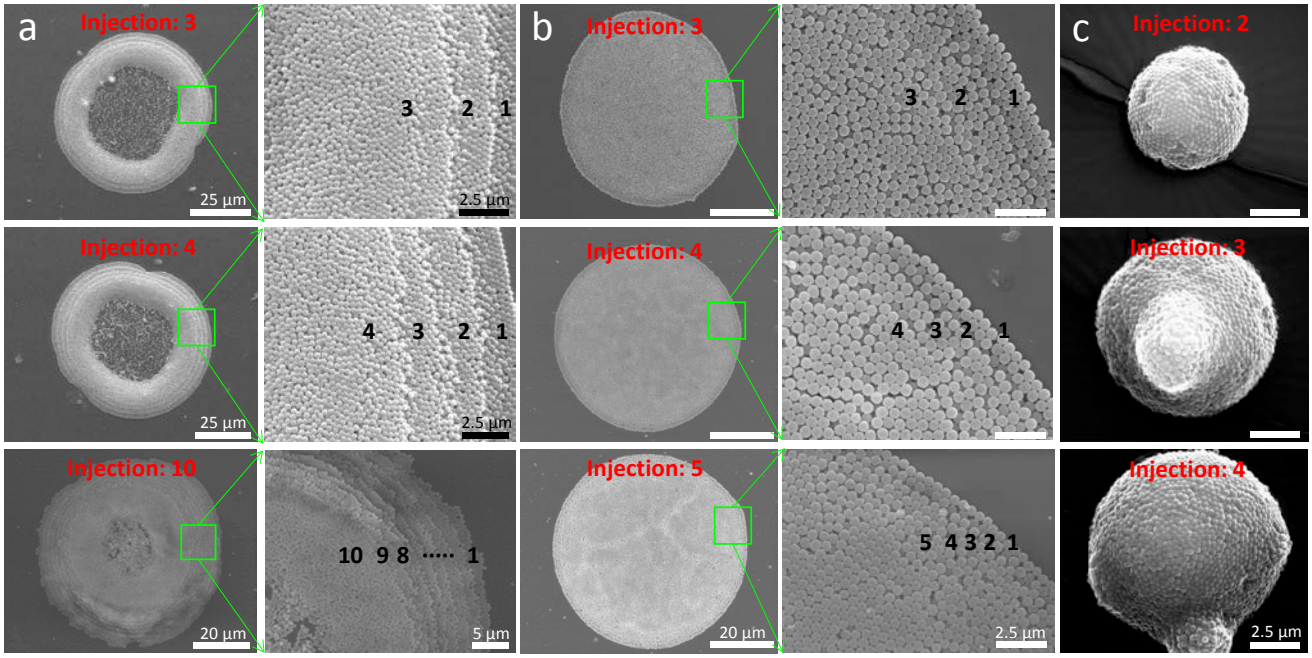

Fig. 3.5 SEM images of multiple injection on glass and PDMS. **a**, Ring-shaped structure with several layers on the glass. **b**, Multi-layered structure composed of individual monolayer. **c**, Dorm-shaped structure on PDMS grow bigger as the number of injection increases.

ULSAN NATIONAL INSTITUTE OF SCIENCE AND TECHNOLOGY

3.3 Coloration of Self-assembled Nanobeads on Various Substrates

Fig. 3.6 shows SAPC patterns of the Nation Treasure No. 1 of Korea (i.e., Namdaemoon) on various substrates with different contact angles, such as slide glass, silicon wafer, polypropylene (PP), and polydimthylsiloxane (PDMS); inset images show contact angles of distilled water droplets. These patterns are assembled in a matrix format by printing droplets with 20% (w/v) nanobead suspension within a 1 cm by 1.5 cm area with a 100 μm spacing distance. By gradually increasing the contact angles of droplets on the substrate, we obtain mono-layered (slide glass, Fig. 3.6a), multi-layered (Si-wafer, Fig. 3.6b) and dome-shaped (PP, Fig. 3.6c) and PDMS, Fig. 3.6d) nanostructures[34]. Next, we captured images using a charge-coupled device (CCD) camera under white light illumination on four samples. Interestingly, mono-layered patterns on hydrophilic surfaces emit iridescent colors, like an opal, and show a rainbow-like pattern at different viewing angles. As printed patterns obtain higher dimensional layers, colorful images no longer appear by forming a photonic band-gap outside the visible spectrum. In other words, the flat structures produced colors while the dome-shaped structures did white lights, implying that the nanostructures have different interaction with incident light.

ULSAN NATIONAL INSTITUTE OF SCIENCE AND TECHNOLOGY

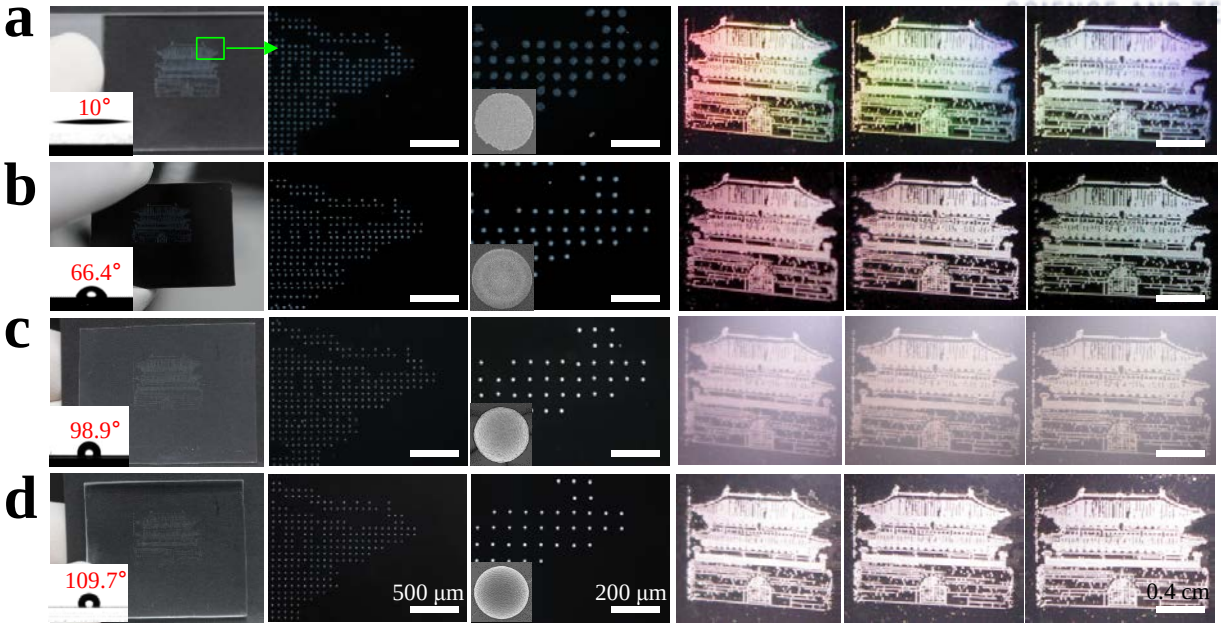

Fig. 3.6 Self-assembly of photonic crystals on various substrates with different contact angles. **a–d**, Comparison of the self-assembly and the structure coloration among difference substrates, such as (a) glass, (b) Si-wafer, (c) polypropylene (PP), and (d) polydimthylsiloxane (PDMS). The patterns on the glass, PP, and PDMS are observed on a black background. A weak light is used for the three images on the left, while a strong light is used for the three images on the right.

ULSAN NATIONAL INSTITUTE OF SCIENCE AND TECHNOLOGY

Chapter 4 Results and Application

4.1 Characterization of Self-assembled Photonic Crystal Patterns

A schematic of an inkjet printing process for producing droplet patterns on a substrate is shown in Fig. 4.1a. Photonic crystals (silica particles) with a 500 nm diameter in injected droplets are self-assembled by drying, resulting in a mono-layered, matrix-format pattern (e.g. dot) on hydrophilic substrates. Water-droplets were mixed with formamide (FA, < 10% v/v) for better self-assembly[18].

We demonstrate an in-series fabrication process for producing structural coloring. Fig. 4.1b shows how various structural colorations are produced in a controlled manner (i–vi). A colorful image (i) needs to be converted to a black and white one (ii); therefore, each pixel (about 100 μm by 100 μm) becomes either black or white (iii). Droplets are then printed on only black pixels, and not on white pixels (iv). For example, we choose an image of Marilyn Monroe and then produce its photonic crystal pattern by injecting ~10,000 droplets into a 1.5 cm by 1.5 cm area. Photographs (Fig. 4.1c) taken of the photonic crystal patterns show various colorations on different backgrounds and in different illumination conditions. The pattern can be not only display under a relatively strong white light illumination on the black background but also hidden under weak illumination regardless of the backgrounds. Notably, it is not easy to detect the pattern even on the black background. In other words, they can be hidden regardless of the illumination strength on a white background, while they can be seen in color or appear whitish on a black background depending on the illumination strength. However, interestingly, clear and colorful images appear under strong illumination and their coloration depends on the viewing angles (Fig. 4.1d).

Fig. 4.2 shows representative photographs of structural colors produced using the same process as Fig. 4.1b: university logo on the left (Fig. 4.2a), and a large-area pattern on the right (Fig. 4.2b).

ULSAN NATIONAL INSTITUTE OF SCIENCE AND TECHNOLOGY

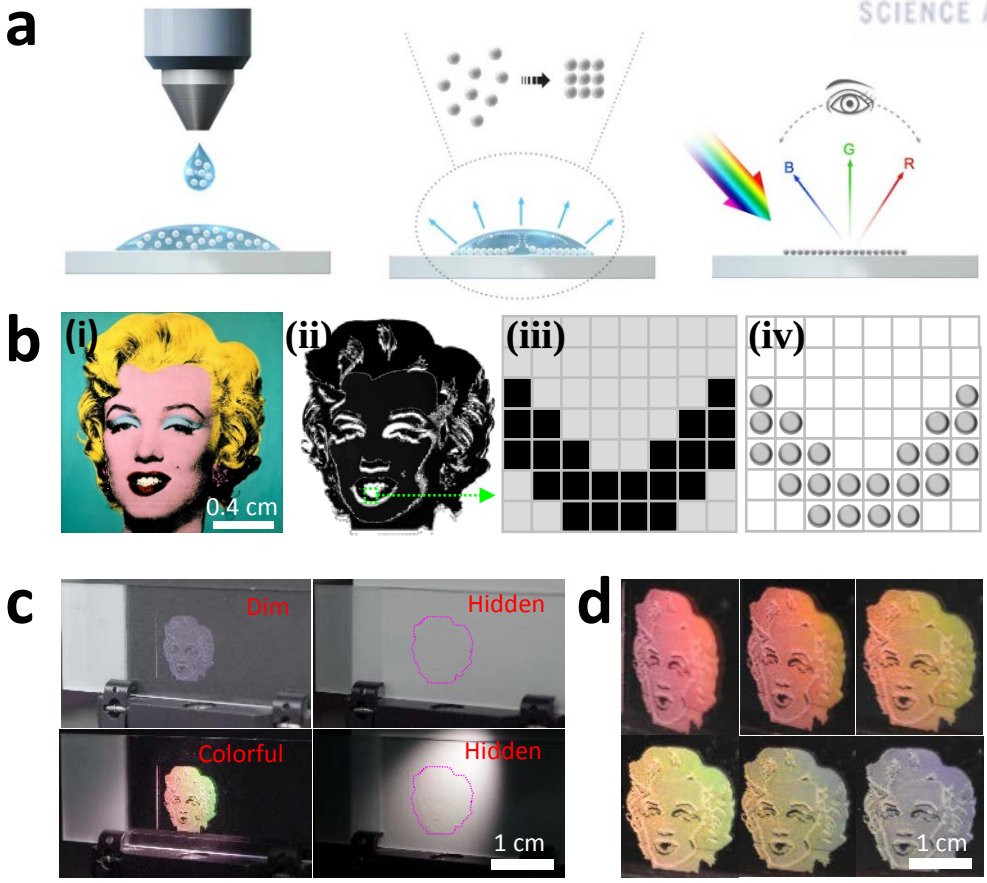

Fig. 4.1 **a**, Schematic of printing and self-assembly of photonic crystals using an inkjet printing technology. **b**, Structure coloration process. A color image (i) is converted to a black and white one (ii). Then, each pixel is determined whether photonic crystals will be injected or not (iii–iv). **c**, The printed patterns can be hidden and shown by manipulating the background and illumination conditions. **d**, Color variation by angle of view.

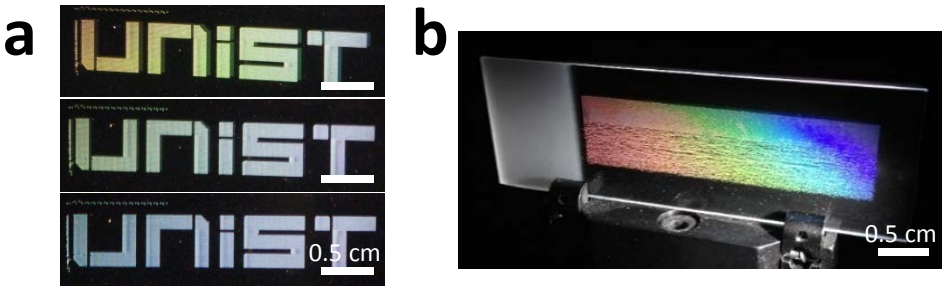

Fig. 4.2 **a-b**, Various images produced using the same structure coloration process exhibit rainbow colors. (a) University logo, (b) large-area pattern.

ULSAN NATIONAL INSTITUTE OF SCIENCE AND TECHNOLOGY

4.2 Theoretical Analysis on Spectra of Mono-layered Photonic Crystals

The structural colors from SAPCs formed on a glass substrate can be directly applied to an anti-counterfeiting system since they are hidden under weak light (daylight) and shown under strong light, which is also well supported by numerical results obtained from the basic diffraction theory of periodic grating structures[31, 35].

We theoretically support structural coloration with a simple diffraction grating model. Fig. 4.3a shows simple periodic elements comprised of SAPC patterns on a hydrophilic surface (mono-layered flat structures). If light composed of rainbow spectra enters the grating elements, spectral components are diffracted into multiple colorful beams in different angular directions. The angles of the diffracted beams are related simply to the periodicity and angle of incident light as shown by Eq. 1. For a plane wave incident at angle θ_i

$$m\lambda = d(\sin\theta_i + \sin\theta_m) \tag{1}$$

where d is the diameter of silica particles, m is the order of the refracted ray, θ_i is the incident angle of light, and θ_m is the angle of refraction relative to the normal plane. The first-order (m = 1) and second-order (m = 2) diffractive beams of photonic crystals with d = 500 nm are obtained by simple numerical calculation, as shown in Fig. 4.3b, c. The first-order diffractive beam is easily detected by the naked eyes, but high-order diffractive beams are imperceptible because they are of shorter wavelengths located in the violet spectrum.

Fig. 4.4 illustrates the experimental setup that defines the position of a light source and a CCD camera by using a spherical coordinate system P(r, θ, ϕ), where r is the distance from the light source or the CCD camera to the origin and θ and ϕ are the angle as defined. Photonic crystal patterns are placed on the y-z plane, and a light source is fixed at θ = 45° on the x-z plane (i.e. P_L(3 cm, 45°, 0°)). These images are obtained by moving the camera at 10° increments from ϕ = -80° to ϕ = 80° on the x-y plane.

ULSAN NATIONAL INSTITUTE OF SCIENCE AND TECHNOLOGY

Fig. 4.5a shows that structural colors of photonic crystal patterns with particles with d = 500 nm gradually change depending on the viewing angle of the camera[36]. The normal angle of the surface (θ_m = 0 and ϕ = 0) shows a violet spectrum. At the surface normal (θ_m = 0 and ϕ = 0), refracted rays have diffracted waves with λ = 392 nm (m = 1), resulting from Eq. (1), thus yielding the violet spectrum imperceptible to human eyes. Furthermore, if we change the position of the camera by changing ϕ along the x-y plane, the diffractive beams provide 2D complex interferences and generate complex, colorful images. For example, diffractive rays at extreme angles of the range we tested (e.g. ϕ = -80° and 80°) produce colorful, rainbow-like patterns covering all visible spectra.

However, if periodicity decreases on a sub-wavelength scale below 400 nm, human eyes cannot sense the diffractive beams of the patterned photonic crystals. Specifically, these patterned photonic crystals with particles with d = 400 nm yield diffractive images with λ = 282.47 nm (m = 1) located at a near-ultraviolet spectrum along normal surfaces and show monochrome images located in a blue spectrum corresponding to the viewing angle of the camera as shown in Fig. 4.5b.

Figs. 4.6-4.8 show photonic crystal images placed on the y-z plane depending on the emitter positions and camera positions, respectively.

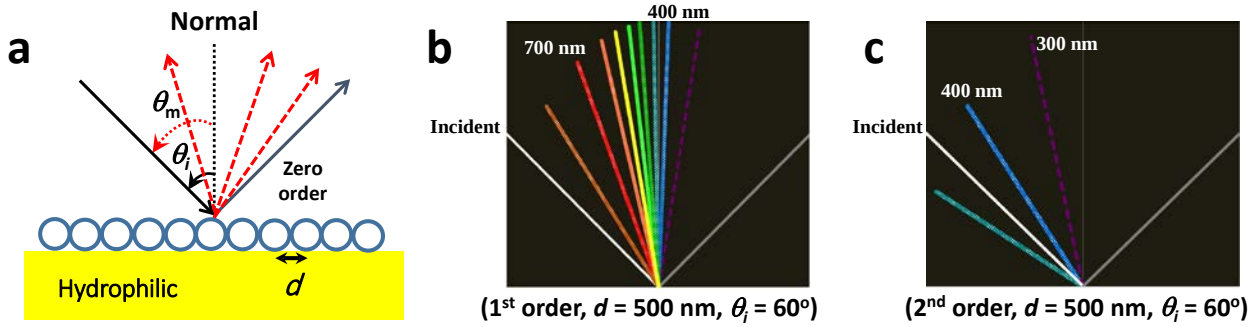

Fig. 4.3 Comparison between theoretical and experimental coloration results from the photonic crystal pattern. **a**, Basic diffraction grating model of mono-layered photonic crystals. **b**, First order diffraction spectrum with incident angle θ_i = 60° and d = 500 nm. **c**, Second order diffraction spectrum with incident angle θ_i = 60° and d = 500 nm.

ULSAN NATIONAL INSTITUTE OF SCIENCE AND TECHNOLOGY

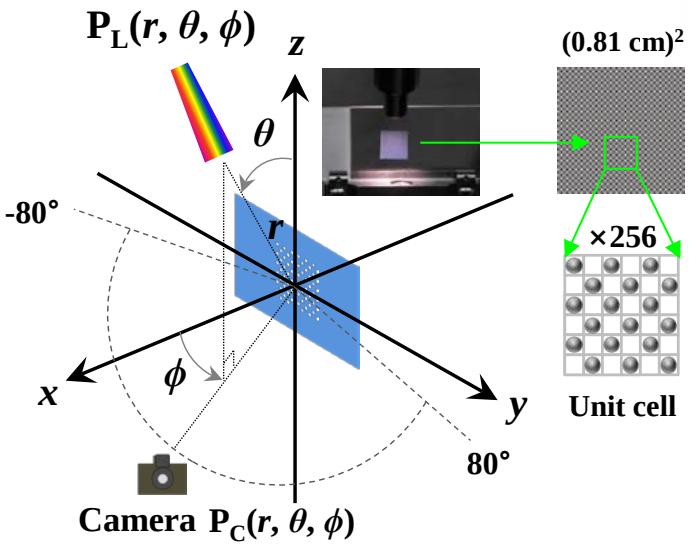

Fig. 4.4 A spherical coordinate system represents the position of incident light P_L (r, θ, ϕ) and that of a CCD camera P_C(r, θ, ϕ).

ULSAN NATIONAL INSTITUTE OF SCIENCE AND TECHNOLOGY

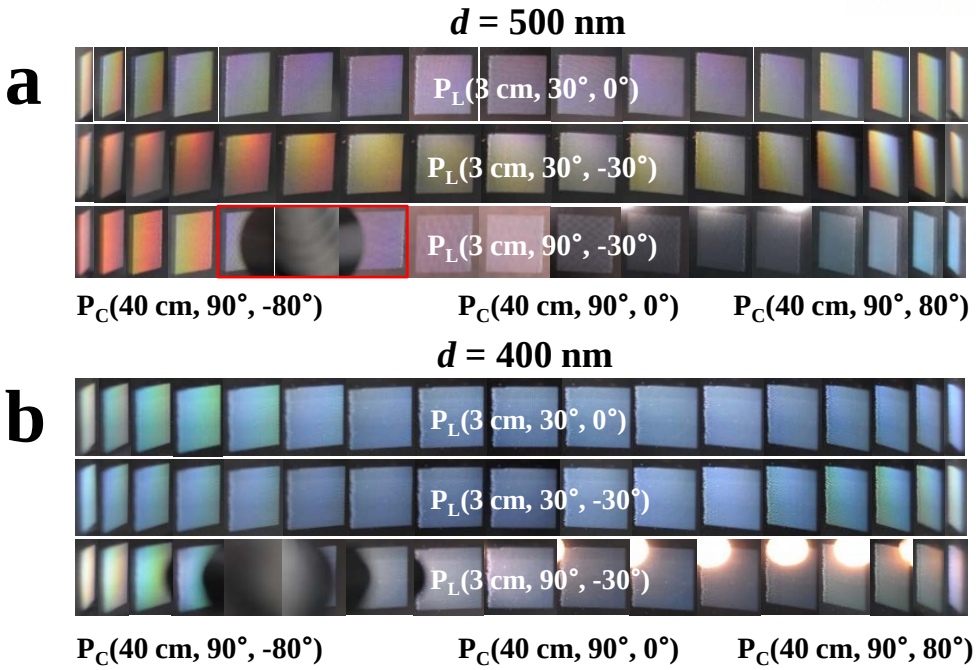

Fig. 4.5 **a**, Photographs of 500 nm photonic crystal patterns when the position of incident light is P_L(3 cm, 30°~90°, 0°) and the camera is placed on the *x*-*y* plane P_C(40 cm, 90°, -80°~80°). **b**, Photographs of 400 nm photonic crystals. The patterns show color variations and significantly depend on viewing angles.

ULSAN NATIONAL INSTITUTE OF SCIENCE AND TECHNOLOGY

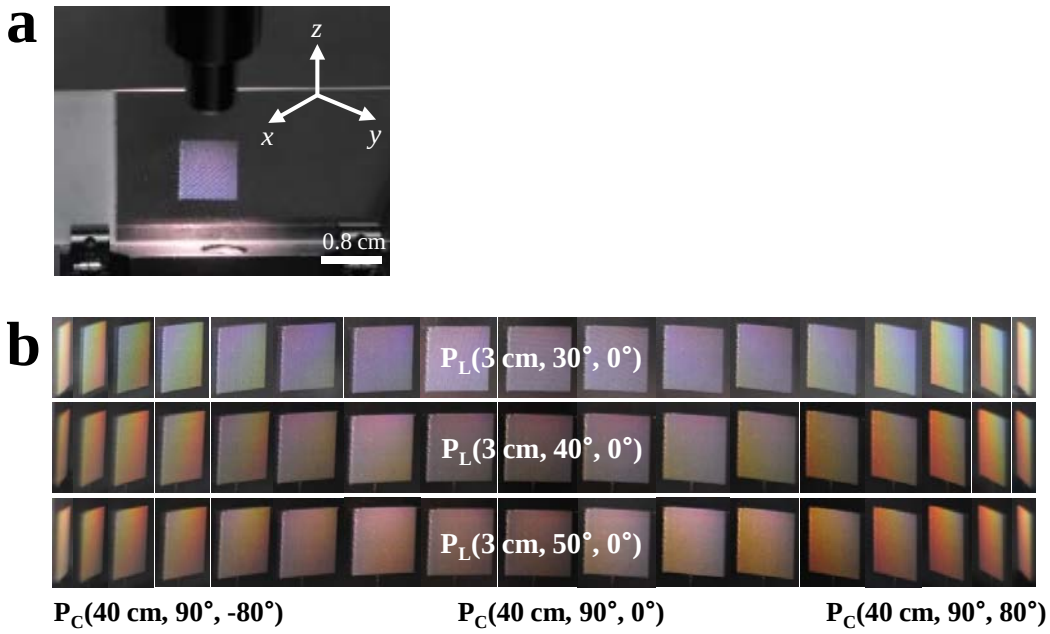

Fig. 4.6 **a**, Position of incident light is P_L(3 cm, 30°~50°, 0°), and the camera is placed on the *x*-*y* plane. **b**, Photographs show color variation as viewing angles change. The color variation is symmetrical with respect to ϕ = 0°. The diameter of the nanobeads is 500 nm.

ULSAN NATIONAL INSTITUTE OF SCIENCE AND TECHNOLOGY

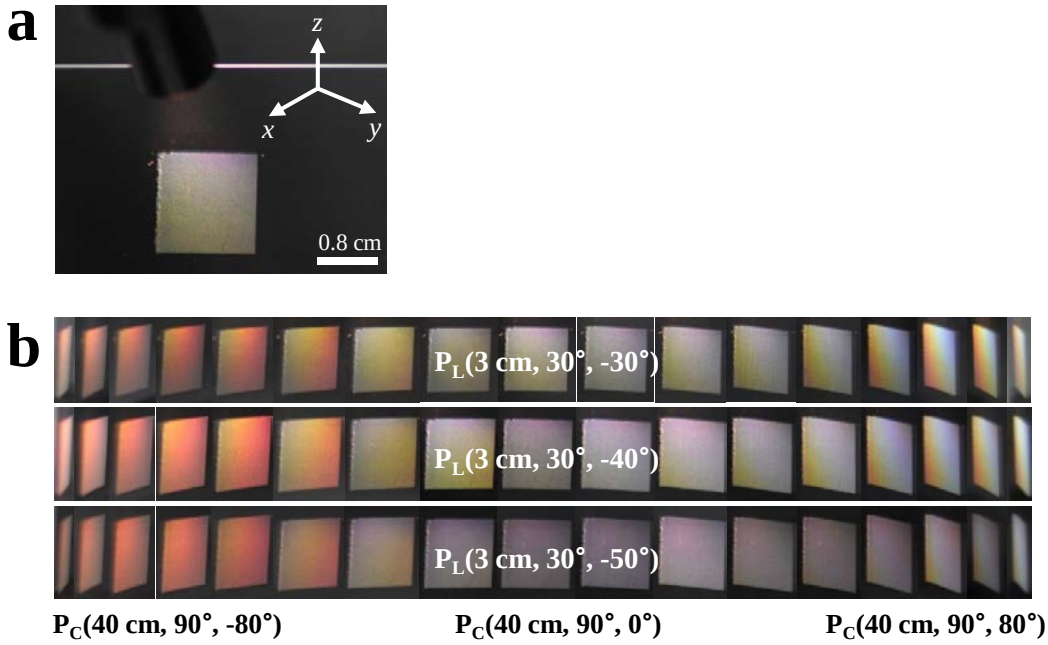

Fig. 4.7 **a**, Position of incident light is P_L(3 cm, 30°, -30~50°), and the camera is placed on the *x*-*y* plane. **b**, Photographs show color variations as viewing angles change. The color variation is asymmetrical with respect to ϕ = 0°. The diameter of the nanobeads is 500 nm.

ULSAN NATIONAL INSTITUTE OF SCIENCE AND TECHNOLOGY

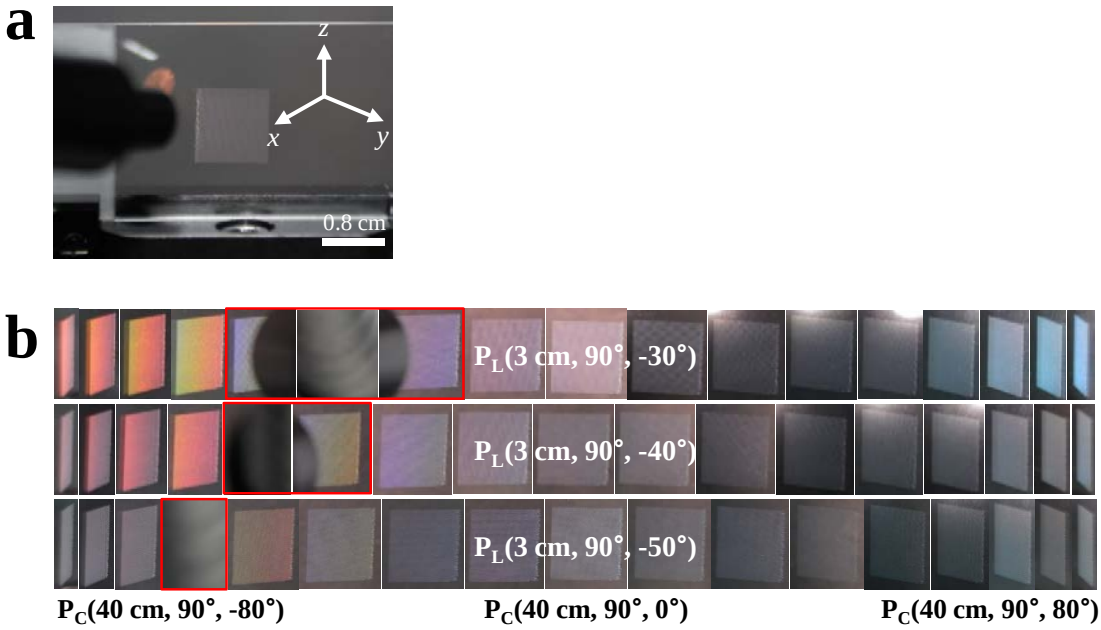

Fig. 4.8 **a**, Position of incident light is P_L(3 cm, 90°, -30°~ -50°), and the camera is placed on the *x*-*y* plane. **b**, Photographs show color variations as viewing angles change. The color variation is asymmetrical with respect to ϕ = 0°. The diameter of the nanobeads is 500 nm.

ULSAN NATIONAL INSTITUTE OF SCIENCE AND TECHNOLOGY

4.3 Spectrum Measurement

In order to quantitatively measure diffraction spectrum, we utilize Agilent's Cary 5000 UV-vis-NIR spectrometer. Fig. 4.9a shows the experimental setup used to obtain diffused and specular reflections. In this experiment, we use the SAPCs with diameters of 500 nm on Si-wafer substrate. Fig. 4.9b and Fig.4.9c show the comparison between diffused and specular reflections. As expected, specular reflection occupy the greater part of reflections. Fig. 4.10 illustrates the diffracted spectrum of s-polarized incident wave with incidence angle θ_i = 60°, 45° and 30°, respectively. When s polarized beam (magnetic field is perpendicular to the plane of incidence) is incident at the angle θ_i = 60°, diffused reflections are measured at θ_m = 30°, 0° and -30° (Fig. 4.10a). Even though diffused reflections are small compared to specular reflections in Fig. 4.9, the diffused reflections depend on wavelength and detection angle θ_m. At θ_m = 30°, the diffused reflection shows the maximum around 600 nm, and at θ_m = 0° and -30°, maximum reflections are located in the blue spectrum. In two other cases (θ_i = 45° and 30°), most diffused reflections appear at the blue light of the visible spectrum (Fig. 4.10b and Fig. 4.10c).

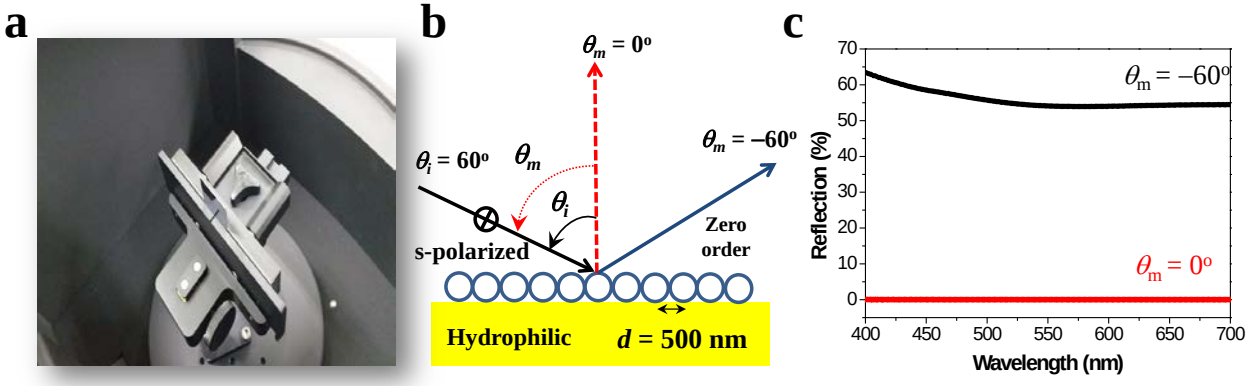

Fig. 4.9 **a**, Experimental setup. Reflection measurement by Agilent's Cary 5000 UV-vis-NIR spectrometer. **b**, Diffraction grating model of mono-layered photonic crystals with incidence angle θ_i = 60°. **c**, Diffused and specular reflections of SAPCs with diameter d = 500 nm when the position of s-polarized incident wave is angle θ_i = 60° and detector is placed on θ_m (0°, -60°).

ULSAN NATIONAL INSTITUTE OF SCIENCE AND TECHNOLOGY

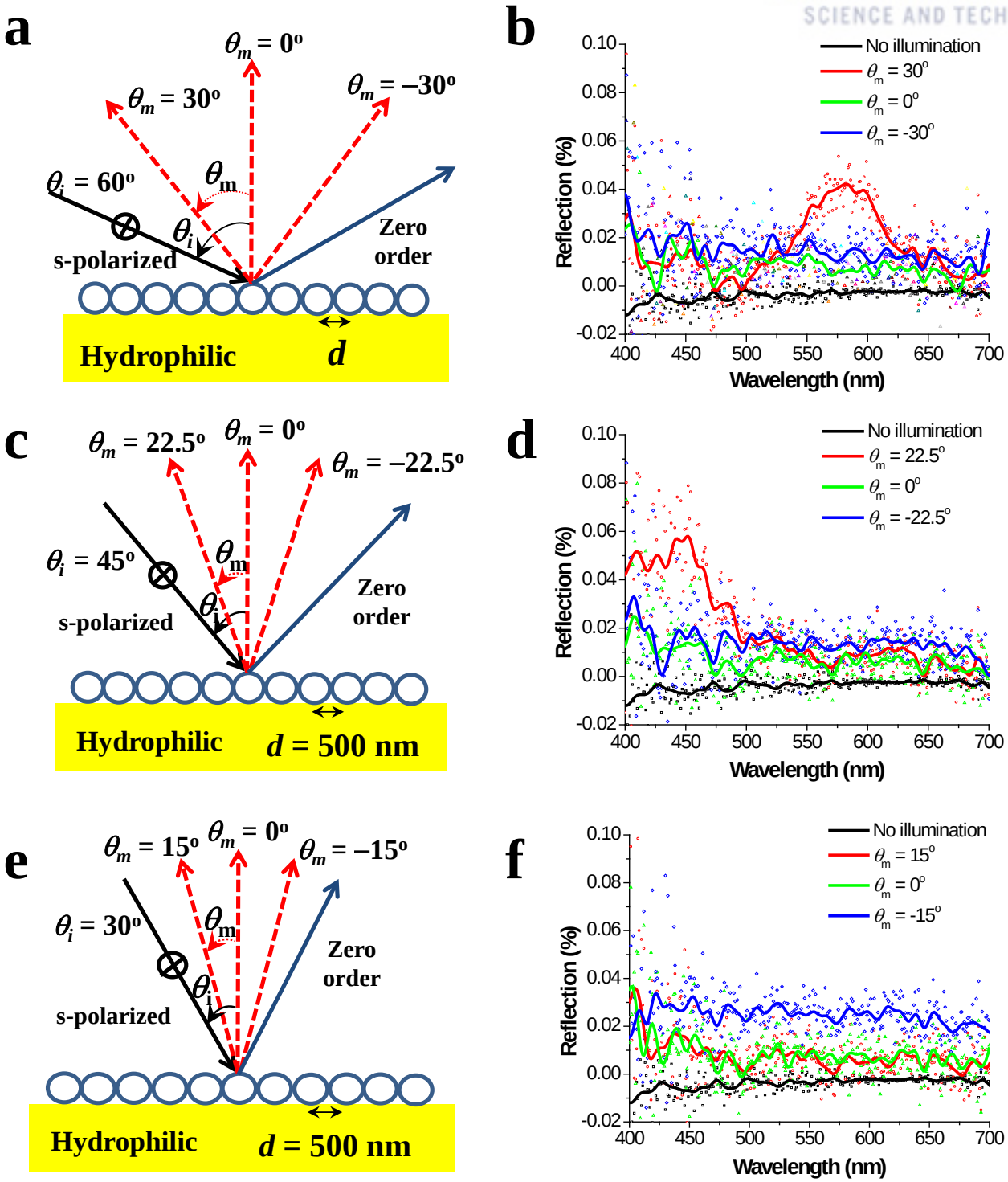

Fig. 4.10 **a**, Diffraction grating model of mono-layered photonic crystals with incidence angle θ_i = 60°. **b**, Diffused reflection measurements of SAPCs with diameter d = 500 nm when the position of s-polarized incident wave is angle θ_i = 60° and detector is placed at three points (θ_m = -30°, θ_m = 0°, and θ_m = 30°). **c**, Diffraction grating model of mono-layered photonic crystals with incidence angle θ_i = 45°. **d**, Diffused reflection measurements of SAPCs with diameter d = 500 nm when the position of s-polarized incident wave is angle θ_i = 45° and detector is placed

ULSAN NATIONAL INSTITUTE OF SCIENCE AND TECHNOLOGY

on θ_m (-22.5°, 0°, 22.5°). **e**, Diffraction grating model of mono-layered photonic crystals with incidence angle θ_i = 30°. **f**, Diffused reflection measurements of SAPCs with diameter d = 500 nm when the position of s-polarized incident wave is angle θ_i = 30° and detector is placed on θ_m (-15°, 0°, 15°).

4.4 Application of SAPCs for Anti-counterfeiting System

As an example of practical applications, we demonstrate anti-counterfeiting system using SAPCs. First, we produce a pattern on an oxygen-plasma-treated PDMS slab with hydrophilic wettability and flexibility (CA = 10° and thickness = 200 μm). The PDMS surfaces are well-attached to glass surface[37]. Interestingly, these patterns can be hidden on a conventional chemical bottle but are detectable with a smartphone light (Fig. 4.11a). Fig. 4.11b shows the same pattern on a glass substrate that can be hidden under daylight, but is visible under strong light, and the color of the pattern is determined by the viewing angle. Fig. 4.11c shows a more realistic counterfeiting application on a paper bill. The pattern is only displayed under a relatively strong illumination. Furthermore, we decrypt the pattern by using commercially available LEDs and a CCD camera, such as a webcam, by fixing the incident angle of light and the reflection angle as shown in Fig. 4.12. In Fig. 4.13, we convert diffractive spectra of three different samples into RGB histograms obtained by 8-bit CCD images. Interestingly, the RGB histograms move to higher intensities with an increase in the number of SAPCs in a unit square area. In addition, the RGB histograms are easily manipulated by changing the location of the detectors. Thus, these SAPCs combined with a light source and a detector show innovative potential for an anti-counterfeiting system to authenticate invaluable and commercial products. Thus, a simple platform comprised of a light source and a detector can decrypt the diffraction pattern of light in terms of optical intensity to produce an RGB histogram[38].

ULSAN NATIONAL INSTITUTE OF SCIENCE AND TECHNOLOGY

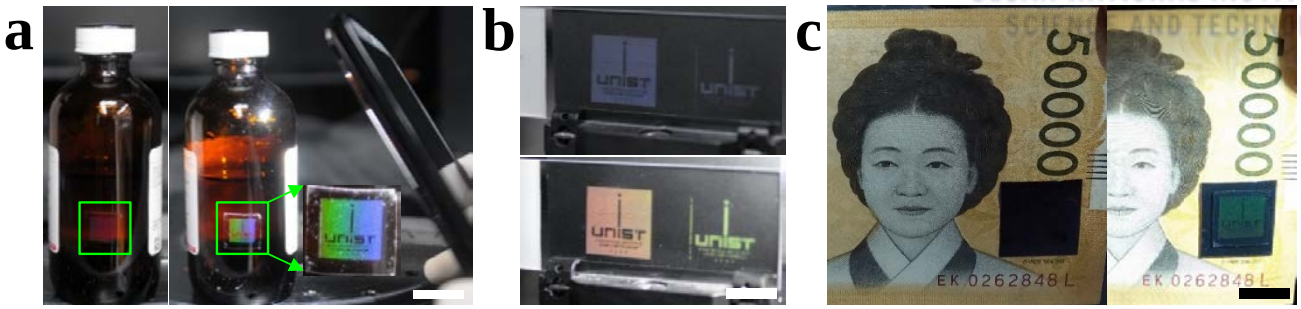

Fig. 4.11 **a**, Photonic crystal patterns showing a logo can be normally hidden, but shown by light illumination using a smartphone. **b**, Images on a glass substrate taken using an iPhone 5 show color variations. **c**, A paper bill with patterns that are normally hidden but can be seen under a bright light.

Fig. 4.12 Credit cards use a hologram as indicated with rectangles in red. Photonic crystal patterns indicated with a rectangle in green appear to replace the hologram.

ULSAN NATIONAL INSTITUTE OF SCIENCE AND TECHNOLOGY

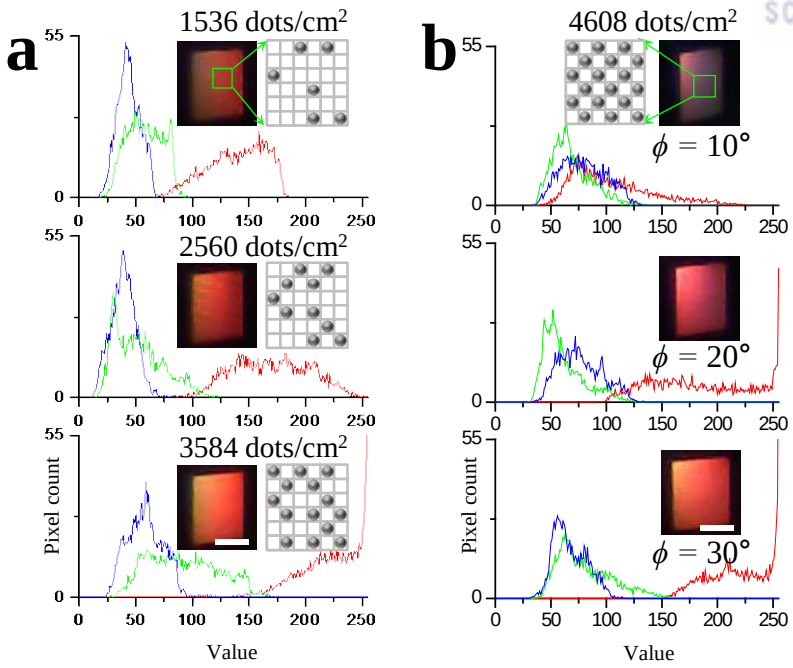

Fig. 4.13 **a**, 8-bit CCD images obtained from different pattern densities show different histograms (Color images taken by a regular smart phone can be split into red, green and blue, respectively.). **b**, The histograms of 8-bit CCD images taken at different viewing angles show significant intensity variation, demonstrating anti-counterfeiting systems.

ULSAN NATIONAL INSTITUTE OF SCIENCE AND TECHNOLOGY

Conclusions

Inkjet printers provide a practical and economical platform to photonic crystal patterns on various substrates by injecting nanobead suspension droplets. The nanobeads in droplets was self-assembled and formed coffee-ring, mono-layered, multi-layered, and dome-shaped nanostructures, respectively. Specifically, 2D self-assembled, mono-layered photonic crystals was developed by utilizing substrate wettability and chemical composition of the silica particle suspension. These patterned photonic crystals (SAPCs) provide stealth ability to avoid pattern detection from counterfeiters under day light illumination and generate multiple colorful holograms on different view angles for complex cryptography. In addition, the number of self-assembled nano-bead arrays in a matrix controls optical intensities, thus yielding extra anti-forgery function. Therefore, the printed photonic-crystal platforms show a practical significance in authentication of invaluable products and could replace conventional systems in an inexpensive and nanotechnological manner.

ULSAN NATIONAL INSTITUTE OF SCIENCE AND TECHNOLOGY

Reference

1. Yablonovitch, E., Inhibited spontaneous emission in solid-state physics and electronics. Physical review letters, 1987. **58**(20): p. 2059.

2. John, S., Strong localization of photons in certain disordered dielectric superlattices. Physical review letters, 1987. **58**(23): p. 2486.

3. Hu, H., et al., Photonic anti-counterfeiting using structural colors derived from magnetic-responsive photonic crystals with double photonic bandgap heterostructures. Journal of Materials Chemistry, 2012. **22**(22): p. 11048-11053.

4. Han, S., et al., Lithographically Encoded Polymer Microtaggant Using High-Capacity and Error-Correctable QR Code for Anti-Counterfeiting of Drugs. Advanced Materials, 2012. **24**(44): p. 5924-5929.

5. Chen, L., et al., The temperature-sensitive luminescence of (Y, Gd) VO4: Bi3+, Eu3+ and its application for stealth anti-counterfeiting. physica status solidi (RRL)-Rapid Research Letters, 2012. **6**(7): p. 321-323.

6. Chiappelli, M.C. and R.C. Hayward, Photonic Multilayer Sensors from Photo-Crosslinkable Polymer Films. Advanced Materials, 2012. **24**(45): p. 6100-6104.

7. Arsenault, A.C., et al., From colour fingerprinting to the control of photoluminescence in elastic photonic crystals. Nature Materials, 2006. **5**(3): p. 179-184.

8. Burgess, I.B., et al., Encoding complex wettability patterns in chemically functionalized 3D photonic crystals. Journal of the American Chemical Society, 2011. **133**(32): p. 12430-12432.

9. Lee, I., et al., Quasi-Amorphous Colloidal Structures for Electrically Tunable Full-Color Photonic Pixels with Angle-Independency. Advanced Materials, 2010. **22**(44): p. 4973-4977.

10. Ge, J., Y. Hu, and Y. Yin, Highly tunable superparamagnetic colloidal photonic crystals. Angewandte Chemie, 2007. **119**(39): p. 7572-7575.

ULSAN NATIONAL INSTITUTE OF SCIENCE AND TECHNOLOGY

11. Campbell, M., et al., Fabrication of photonic crystals for the visible spectrum by holographic lithography. Nature, 2000. **404**(6773): p. 53-56.

12. Jeon, S., et al., Fabricating three-dimensional nanostructures using two photon lithography in a single exposure step. Optics Express, 2006. **14**(6): p. 2300-2308.

13. Cumpston, B.H., et al., Two-photon polymerization initiators for three-dimensional optical data storage and microfabrication. Nature, 1999. **398**(6722): p. 51-54.

14. Kawata, S., et al., Finer features for functional microdevices. Nature, 2001. **412**(6848): p. 697-698.

15. Deubel, M., et al., Direct laser writing of three-dimensional photonic-crystal templates for telecommunications. Nature materials, 2004. **3**(7): p. 444-447.

16. Gratson, G.M., M. Xu, and J.A. Lewis, Microperiodic structures: Direct writing of three-dimensional webs. Nature, 2004. **428**(6981): p. 386-386.

17. Cheng, C.-C. and A. Scherer, Fabrication of photonic band-gap crystals. Journal of Vacuum Science & Technology B, 1995. **13**(6): p. 2696-2700.

18. Park, J. and J. Moon, Control of colloidal particle deposit patterns within picoliter droplets ejected by ink-jet printing. Langmuir, 2006. **22**(8): p. 3506-3513.

19. Cui, L., et al., Fabrication of large-area patterned photonic crystals by ink-jet printing. Journal of Materials Chemistry, 2009. **19**(31): p. 5499-5502.

20. Wang, L., et al., Inkjet printed colloidal photonic crystal microdot with fast response induced by hydrophobic transition of poly (N-isopropyl acrylamide). Journal of Materials Chemistry, 2012. **22**(40): p. 21405-21411.

21. Choi, W.S., et al., Synthetic multicellular cell-to-cell communication in inkjet printed bacterial cell systems. Biomaterials, 2011. **32**(10): p. 2500-2507.

ULSAN NATIONAL INSTITUTE OF SCIENCE AND TECHNOLOGY

22. Jeong, S., et al., Controlling the thickness of the surface oxide layer on Cu nanoparticles for the fabrication of conductive structures by ink-jet printing. Advanced Functional Materials, 2008. **18**(5): p. 679-686.

23. Kim, D., et al., Direct writing of silver conductive patterns: Improvement of film morphology and conductance by controlling solvent compositions. Applied Physics Letters, 2006. **89**(26): p. 264101.

24. de Gans, B.J. and U.S. Schubert, Inkjet Printing of Polymer Micro-Arrays and Libraries: Instrumentation, Requirements, and Perspectives. Macromolecular rapid communications, 2003. **24**(11): p. 659-666.

25. Wikipedia. Inkjet printing. 2015; Available from: http://en.wikipedia.org/w/index.php?title=Inkjet_printing&oldid=640581926.

26. de Gans, B.J., P.C. Duineveld, and U.S. Schubert, Inkjet printing of polymers: state of the art and future developments. Advanced materials, 2004. **16**(3): p. 203-213.

27. ; Available from: http://www.paperandprint.com/digital-printer/features/dp-2013/september-2013/20-19-13-all-in-the-head.aspx#.VFxTgPmsVBk.

28. Inkjet printer DMP-2800 series User Manual, Fujifilm Dimatix,Inc. .

29. opalux. the leader in photonic color technology. 2015; Available from: http://opalux.com/.

30. Hu, H., et al., Invisible photonic printing: computer designing graphics, UV printing and shown by a magnetic field. Scientific reports, 2013. **3**.

31. Yao, J., et al., Selective appearance of several laser-induced periodic surface structure patterns on a metal surface using structural colors produced by femtosecond laser pulses. Applied Surface Science, 2012. **258**(19): p. 7625-7632.

32. Deegan, R.D., et al., Capillary flow as the cause of ring stains from dried liquid drops. Nature, 1997. **389**(6653): p. 827-829.

33. Hu, H. and R.G. Larson, Marangoni effect reverses coffee-ring depositions. The Journal of Physical Chemistry B, 2006. **110**(14): p. 7090-7094.

ULSAN NATIONAL INSTITUTE OF SCIENCE AND TECHNOLOGY

34. Li, Y., et al., Nanoparticle-tuned spreading behavior of nanofluid droplets on the solid substrate. Microfluidics and Nanofluidics: p. 1-10.

35. Yeh, S.L. and S.T. Lin, Identifying a dot-matrix hologram by checking the intersecting angles of its gratings. Optics Communications, 2010. **283**(2): p. 243-248.

36. Tang, M., et al., Angle coder of anti-counterfeiting color in optical micro-mirror arrays. Optik-International Journal for Light and Electron Optics, 2013. **124**(23): p. 6146-6148.

37. Bhattacharya, S., et al., Studies on surface wettability of poly (dimethyl) siloxane (PDMS) and glass under oxygen-plasma treatment and correlation with bond strength. Microelectromechanical Systems, Journal of, 2005. **14**(3): p. 590-597.

38. Ecker, M. and T. Pretsch, Multifunctional poly (ester urethane) laminates with encoded information. RSC Advances, 2014. **4**(1): p. 286-292.

ULSAN NATIONAL INSTITUTE OF SCIENCE AND TECHNOLOGY

Acknowledgement

By the time of completing this thesis, I would like to thank many people who supported me during my study in UNIST.

First of all, I wish to express my sincerest gratitude to my supervisor, Prof. Taesung Kim for his tutoring and continuous encouragement which he has given me during the last two years. His technical and editorial advice was essential to the completion of this thesis.

I would also like to thank my committee members, Prof. Tasesung Kim, Prof. Myounghoon Song, and Dr. Kyungjun Song for serving as my committee members.

I am thankful to present and past members of the μFNM lab: Kim Minseok, Lim Jiwon, Lee Jongwan, Mingie Jia, Ha Dogyeong, Park Jungsik and undergraduate students.

Finally I want to thank my heartfelt gratitude to my family. My parents, Mr. Nam and Mrs. Kwak, have always been my strongest supporters. I also want to thank my sister's family, Nam Minyoung and Hyun Jinwoo, and friends who encouraged me to keep going.